DENTAL MATERIALS 35 (2019) e97–e106

Available online at www.sciencedirect.com

ScienceDirect

journal homepage: www.intl.elsevierhealth.com/journals/dema

Effect of the volume fraction of zirconia suspensions on the microstructure and physical properties of products produced by additive manufacturing

Kyoung-Jun Jang[a], *Jin-Ho Kang*[a], *John G. Fisher*[b], *Sang-Won Park*[a,*]

[a] *Department of Prosthodontics, School of Dentistry, Chonnam National University, Gwangju 61186, Republic of Korea*

[b] *School of Materials Science and Engineering, Chonnam National University, Gwangju, 61186, Republic of Korea*

ARTICLE INFO

Article history:
Received 9 October 2018
Received in revised form
18 January 2019
Accepted 4 February 2019

Keywords:
Additive manufacturing
Zirconia 3D printing
Rapid prototyping
DLP (digital light processing)
Zirconia suspension
Zirconia photopolymer resin

ABSTRACT

Objective. The objectives of the present study were: (1) to analyze the dispersion and optical properties of suspensions with various volume fractions of zirconia, and (2) to assess the influence of zirconia volume fraction on the microstructure and physical properties of products produced by the additive manufacturing and sintering process.

Methods. Zirconia specimens were fabricated by an additive manufacturing technique using a DLP (digital light processing) system. The zirconia suspensions were divided into six groups based on zirconia volume fraction within the range of 48–58 vol%.

Results. The maximum volume fraction of zirconia in suspensions possible for printing was 58 vol%. The cure depth of the zirconia suspensions decreased as the volume fraction increased. The cure depth was greater than 100 μm after 15 s photocuring in all groups. Geometrical overgrowth tended to increase gradually as the volume fraction of zirconia increased within the range of 28.55–36.94%. The 3-point bending strength of the specimens increased as the volume fraction of zirconia in the suspension increased, reaching a maximum value of 674.74 ± 32.35 MPa for a volume fraction of 58 vol%. Cracks were observed on the surfaces of zirconia specimens and these cracks increased in number as zirconia volume fraction decreased.

Significance. In this experiment, the viscosity of zirconia suspensions sharply increased from a volume fraction of 54 vol%. Because of the very high viscosity, 58 vol% was the maximum volume fraction possible for additive manufacturing. After polymerization, all specimens showed some distortion due to geometrical overgrowth. The maximum 3-point bending strength was 674.74 ± 32.35 MPa for a volume fraction of 58 vol%. But the maximum strength of sintered zirconia prepared by additive manufacturing is inferior to that of conventionally sintered zirconia.

* *Corresponding author.*
E-mail addresses: zircong@naver.com (K.-J. Jang), dldigh8901@gmail.com (J.-H. Kang), johnfisher@jnu.ac.kr (J.G. Fisher), psw320@chonnam.ac.kr (S.-W. Park).

https://doi.org/10.1016/j.dental.2019.02.001

1. Introduction

Zirconia prostheses, either pre-sintered or fully-sintered, are mechanically processed using CAD/CAM (Computer Aided Design/Computer Aided Manufacturing) systems [1,2]. However, zirconia prostheses mechanically processed using CAD/CAM tend to have rough scratches or defects on their surfaces, leading to cracks and making them vulnerable to fracture. Furthermore, processing into complex shapes is difficult [3–5].

Additive manufacturing has been introduced as a highly precise method in the field of dentistry [6,7]. It became possible to use polymerization processes for additive manufacturing, such as SLA (stereolithography) and DLP (digital light processing), to build layers of materials with precision, excellent surface quality and fast printing speed [8–14]. SLA uses a laser to cure the thin layer of slurry. The DLP system uses a light mask created by a digital micro mirror device to cure the entire layer simultaneously.

However, zirconia is difficult to print by additive manufacturing techniques due to its low flowability with high concentration of zirconia, strong light scattering and high refractive index [15]. Since the refractive index of zirconia is 20–27% higher than that of other ceramic materials such as silica and alumina, it can cause significant scattering of the incident light during photopolymerization. As a result, the cure depth of the photo polymer is limited [16–18].

Recent studies have focused on improving the photocuring properties of layered products for ceramics produced by SLA or DLP systems [19–21]. In general, ceramic powder, photosensitive resins, dispersant and other additive agents are mixed for the suspensions. Ceramic suspensions require a sufficient solids volume fraction for high density, strength and shrinkage control [22–25]. And effective dispersion of the ceramic powder can create uniform layers and reduces defects accordingly. In addition, the cure depth and low light scattering are important because sufficient cure depth and low light scattering are needed for good physical properties of the final products [26].

Zirconia products fabricated by photopolymerizing techniques cannot have sufficient strength or sintering properties when low volume fractions of solid components are used. The objectives of the present study were: (1) to analyze the dispersion and optical properties of suspensions with various volume fractions of zirconia, and (2) to assess the influence of volume fraction on the microstructure and physical prop-

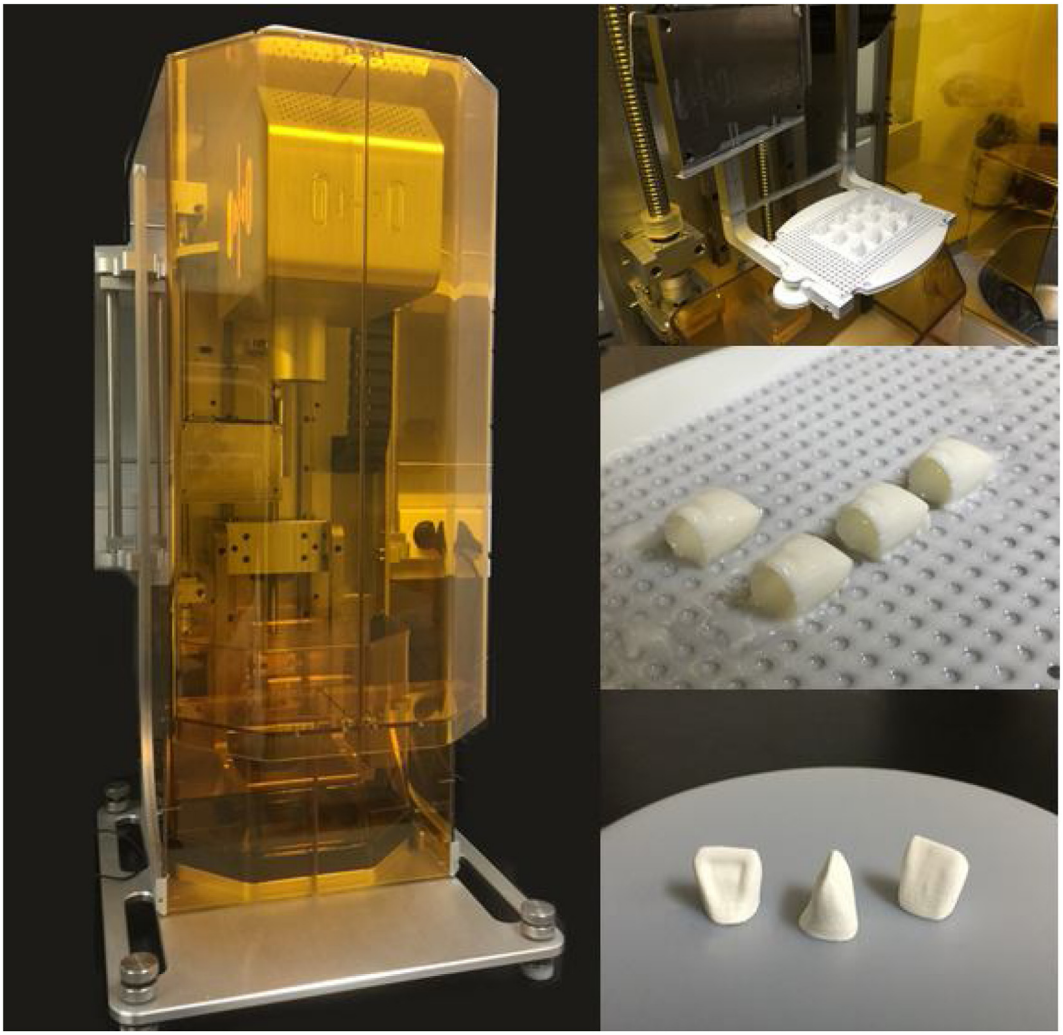

Fig. 1 – Top–down DLP 3D printer for zirconia additive manufacturing.

Table 1 – Physicochemical properties of materials for zirconia suspension.

Materials	Density (g/mL)	Refractive index (325 nm)	Viscosity (mPas, 25 °C)
Zirconia	6.05	2.15	–
HDDA[a]	1.02	1.45	9
IBA[b]	0.98	1.47	8
PNPGDA[c]	1.00	1.44	15
Photoinitiator	0.52–2.48	–	–
Dispersant	–	–	–

[a] HDDA: 1,6-hexanediol diacrylate.
[b] IBA: isobomyl acrylate.
[c] PNPGDA: propoxylated neopentyl glycol diacrylate.

Table 2 – Experiment groups used in this study.

Group	Zirconia	Acrylate	Photoinitiator	Dispersant	Total (vol%)
48	48.00	38.39	0.16	13.45	100
50	50.00	35.84	0.15	14.01	100
52	52.00	33.29	0.14	14.57	100
54	54.00	30.75	0.13	15.13	100
56	56.00	28.20	0.12	15.68	100
58	58.00	25.64	0.11	16.25	100

erties of specimens produced by the additive manufacturing and sintering processes.

2. Materials and methods

2.1. *Additive manufacturing*

The DLP 3D printer (Octave Light R1, Octave Light Ltd., Hong Kong) used in this study has a top–down mechanism (Fig. 1). In this DLP, radical photopolymerization can be selectively performed in a wavelength range of 350–450 nm. The layer thickness was set at 25 μm. The size of the printer build plate is 75.6 mm (length) × 134.4 mm (width) × 186 mm (height). The x, y resolution of the DLP is 70 μm × 70 μm per pixel. The temperature of the suspension was maintained at a room temperature of 25 °C. The 3D printer was calibrated before the experiment using an STL file provided by the company and the subjects were printed directly on the build plate.

2.2. *Fabrication of zirconia photopolymer suspensions*

The zirconia suspensions were mixed with 3 mol% Y_2O_3 stabilized zirconia powder (TZ-3Y, Tosoh, Japan), acrylates (1,6-hexanediol diacrylate, isobornyl acrylate, propoxylated neopentyl glycol diacrylate, Sigma Aldrich, USA), photo initiators (Irgacure 819, Ciba Specialty Chemicals, Inc., Switzerland) and dispersant (BYK-180, BYK Chemie, GmbH, Wesel, Germany). Dispersant is added for stabilization of the suspensions and prevention of sedimentation of the zirconia. Physicochemical properties of each material are summarized (Table 1). Specimens were divided into six groups based on zirconia volume fraction in the range of 48–58 vol% (Table 2). A planetary centrifugal mixer (ARV-310, Thinky Corp., Japan) was used for homogenous mixing under vacuum for 20 min.

2.3. *Composition of zirconia photopolymer suspensions*

2.3.1. *Rheological measurement*

The viscosity of each suspension (n = 10) was measured at a shear rate of 5/s using a rheometer (DV3T, Brookfield Engineering Laboratories, Stoughton, MA, USA) (ISO-2555) [27].

2.3.2. *Measurement of the cure depth (Cd) and geometrical overgrowth*

The cure depth of zirconia suspensions (n = 10) was determined by operating the DLP at a distance of 20 cm for 1–30 s with UV light (375–425 nm, UVA range) at a uniform intensity of 30 mW/cm^2, to establish sufficient curing time while layers were stacked. Light scattering effects can cause larger areas to cure than the area actually proposed. The geometrical overgrowth was measured on the holes of a printed specimen by subtracting the original diameter of 250 μm (Fig. 2). The cured specimens were rinsed and their sizes were measured with an optical microscope (AD7013MZT, Dino-Lite, New Taipei City, Taiwan) with image analysis software (Image J, National Institutes of Health, USA).

2.4. *Thermal analysis and thermal treatment for debinding and sintering*

Thermal analysis was performed for debinding of printed specimens (solid objects). Specimens were heated in a thermal analyzer (SDT Q600, TA Instruments, Surrey, UK) in standard air atmosphere up to 1450 °C at a rate of 2.5 °C/min (ISO-11358) [28]. The final sintering schedule was performed according to the thermal analysis results.

2.5. *Linear sintering shrinkage and density*

For linear shrinkage, the length before and after sintering (n = 10) was measured using a micrometer caliper (Fig. 3(a)). Three measurements were made for each specimen and linear

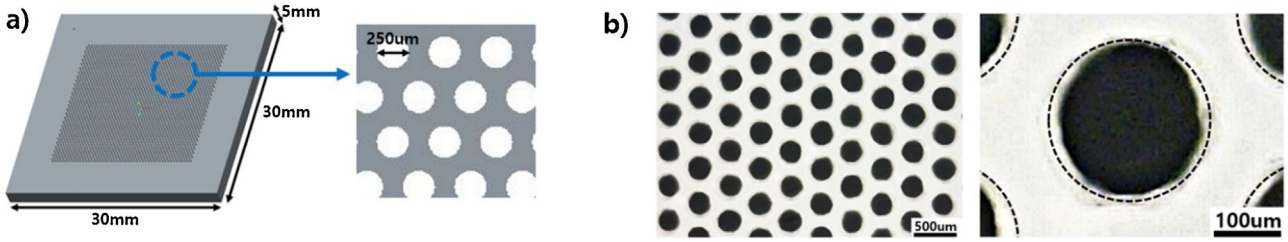

Fig. 2 – Schematization of the STL file of zirconia specimen and the effect of geometrical overgrowth (a) The x, y, z dimension of test specimen and hole (250 μm in diameter) for geometrical overgrowth measurement and (b) deformed hole form in printed product due to the scattering of light.

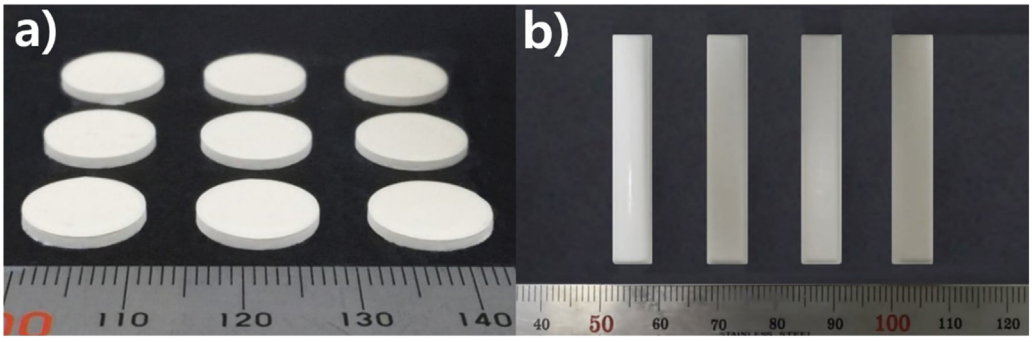

Fig. 3 – The specimens preparation for (a) linear shrinkage and density, (b) 3-point bending strength measurement.

shrinkage was calculated according to ASTM C326 [29]. Relative density was calculated by measuring the volume density of each specimen (n = 10) according to the Archimedes principle (ISO-18754) [30].

2.6. 3-point bending strength

The 3-point bending strength was measured by using a universal testing machine (RB Model 301, R&B, Daejeon, Korea) (ISO-6872) [31]. A load was applied at the center of the supporting point of the specimens (n = 10) at a crosshead speed of 0.5 mm/min until the specimens started to crack (Fig. 3(b)). The value of the load (N) at which the specimens cracked was recorded.

2.7. X-ray diffraction (XRD) analysis

X-ray diffraction (X'pert PRO, Panalytical, Eindhoven, Netherlands) analysis was performed on as-sintered specimens in each group using Cu-Kα X-rays at a scan rate of 5°/min within the range of 20–80°.

2.8. Microstructural analysis

Defect analysis of specimens prepared from suspensions with various solid loadings of zirconia (vol%) were performed using a microscope (IS 300, Olympus, Tokyo, Japan). Microstructures were observed with a scanning electron microscope (JSM-7500F FE-SEM, JEOL, Tokyo, Japan) (ISO-13356) [32].

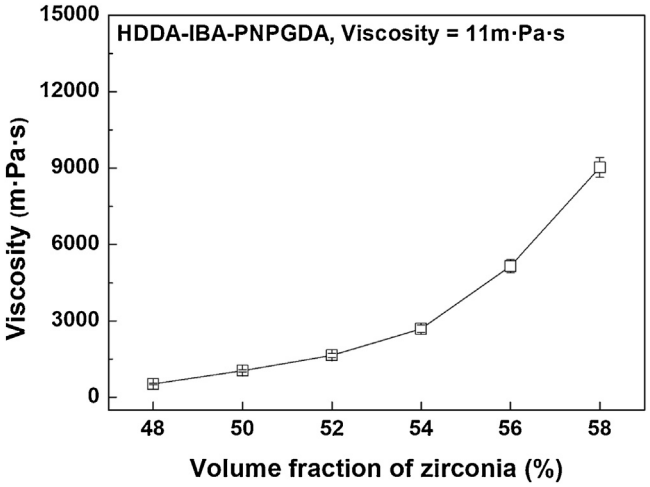

Fig. 4 – The viscosity of zirconia suspension according to volume fraction.

3. Results

3.1. Viscosity

A highest viscosity of 9025 ± 57 m Pa s was measured at the highest volume fraction of 58 vol% (Fig. 4). The volume fraction of the suspension for which it is possible to observe the flow with the naked eye was up to a solids loading of 54 vol%. And the flow ability of the zirconia suspension was drastically decreased from the solids loading of more than 56 vol%. The

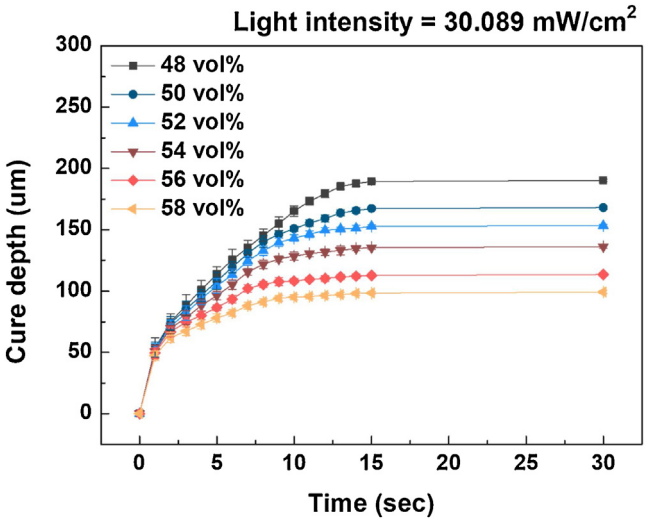

Fig. 5 – The cure depth according to curing time in the different volume fraction of zirconia.

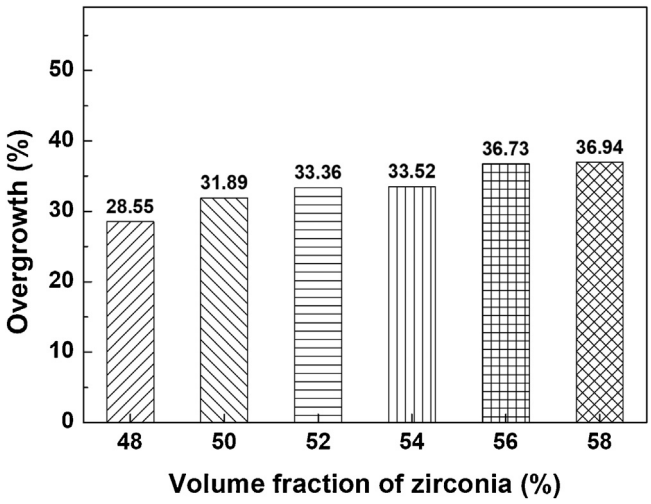

Fig. 6 – The geometrical overgrowth according to the volume fraction of zirconia.

maximum volume fraction possible for printing was 58 vol% in this study.

3.2. *Cure depth*

The cure depths of each zirconia volume fraction according to photocuring time were measured (Fig. 5). The cure depth tended to decrease as cure time decreased and volume fraction increased. After 15 s of photocuring time, all specimens cured completely. The maximum cure depth in each volume fraction in order of decreasing volume fraction after 30 s of photocuring was 99.28 ± 1.27, 113.57 ± 1.33, 136.26 ± 1.38, 153.27 ± 1.24, 168.04 ± 1.32, and 190.24 ± 1.08 μm.

3.3. *Geometrical overgrowth*

Geometrical overgrowth tended to increase gradually as the volume fraction of zirconia increased (Fig. 6). The minimum geometrical overgrowth of 28.55% was observed in the group with a volume fraction of 48 vol%. The maximum geometrical overgrowth of 36.94% was observed with a volume fraction of 58 vol%.

3.4. *Thermal analysis and thermal treatment*

Debinding steps were observed at temperature of 200, 300 and 500 °C (Fig. 7). All organic binders were removed below 600 °C under air atmosphere. The final sintering step was performed at 1450 °C. Drying, debinding and sintering were scheduled according to Fig. 8.

3.5. *Linear sintering shrinkage rate and relative density*

The lowest relative density (83.02%) and the highest linear shrinkage rate (23.81%) were found in the group with volume fraction of 48 vol%. Relative densities of samples prepared from suspensions with volume fractions of 56 vol% and 58 vol% were 91.65% and 92.79% and their linear sintering shrinkages were 19.85% and 19.37%, respectively (Fig. 9).

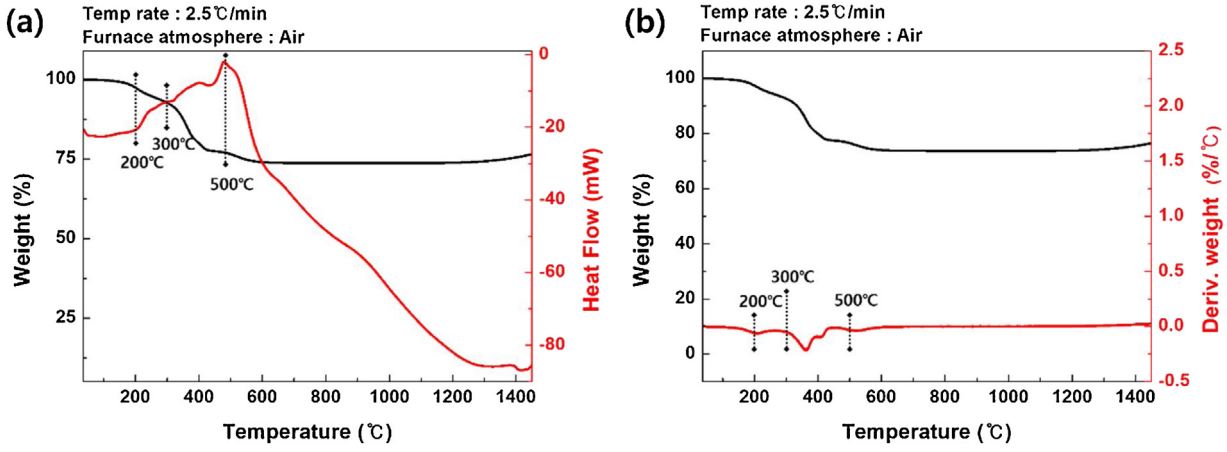

Fig. 7 – Comparison between heat flow (a) and derivative weight (b) curves of green body specimens up to 1450 °C.

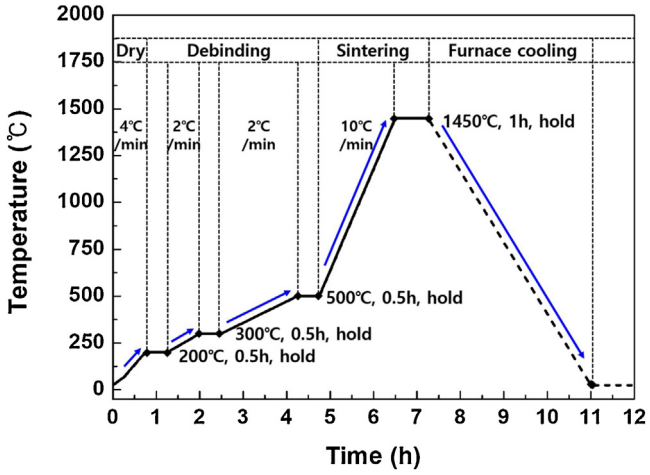

Fig. 8 – Thermal treatment for drying, debinding, and sintering of green body specimens.

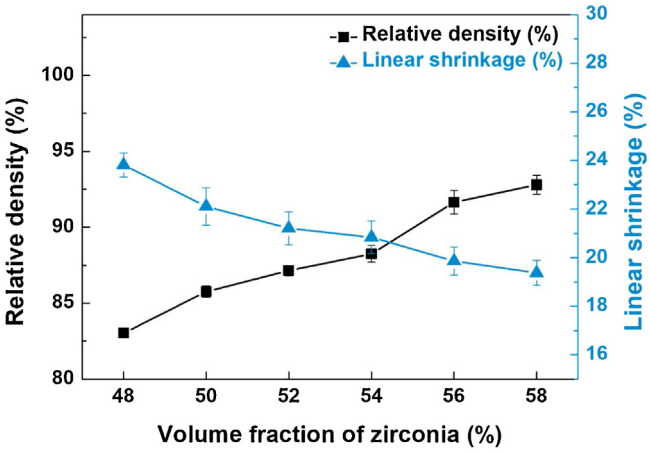

Fig. 9 – The relative density and linear shrinkage values for different volume fraction of zirconia.

3.6. *Mechanical properties (3-point bending strength)*

The lowest strength (94.25 ± 17.29 MPa) was observed in the group with a volume fraction of 48 vol%. The highest increasing rate of strength between groups was 45.91% and it was observed between groups of 50 vol% and 52 vol%. The highest strength was 674.74 ± 32.35 MPa in the group with a volume fraction of 58 vol% (Fig. 10).

3.7. *X-ray diffraction (XRD) analysis*

Results showed peaks of 2θ at 30.2°, 34.7°, and 35.2° corresponding to characteristic planes (101)t, (002)t, and (110)t of t-ZrO_2, respectively. The amount of m-ZrO_2 was below the detection limit in all specimens (Fig. 11).

3.8. *Microstructural analysis*

Cracks were observed on the surface of sintered specimens in (a)–(c) which had relatively low volume fractions (Fig. 12).

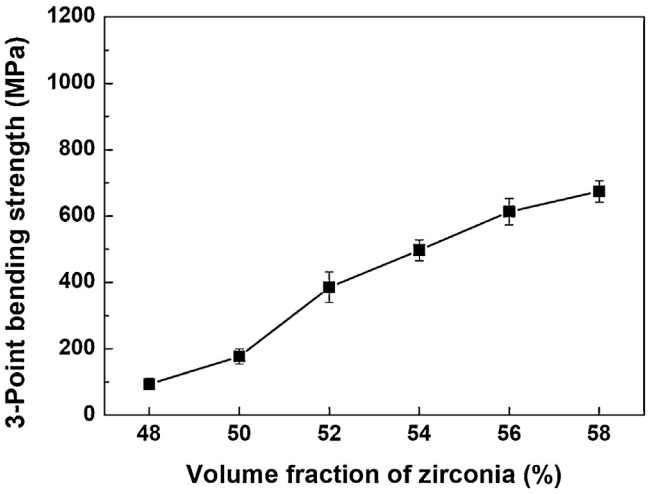

Fig. 10 – The 3-point bending strength of sintered specimens according to volume fraction.

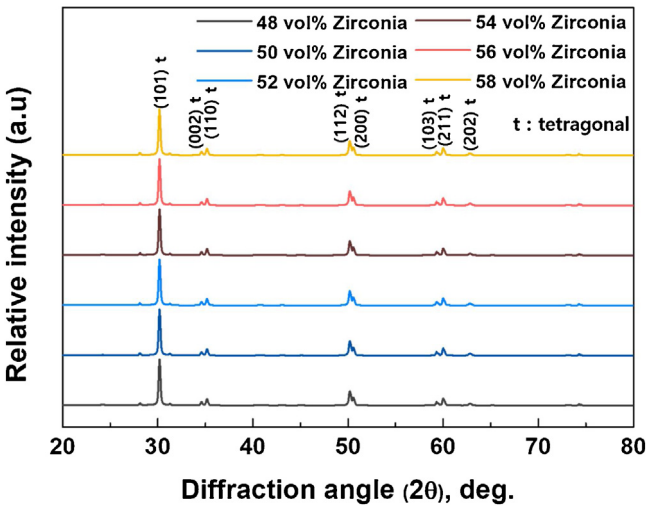

Fig. 11 – The XRD patterns of sintered specimens for different volume fraction of zirconia.

These cracks increased in number as zirconia volume fraction decreased.

In cross sectional images, repeat layers with thickness of 25 μm were observed in green bodies of all groups. In addition, the defects marked with arrows increased in number as the zirconia volume fraction decreased (Fig. 13(a)). After sintering, repeat layers and defects were no longer visible (Fig. 13(b)).

4. Discussion

The characteristics of the ceramic suspension are very important for the DLP-based additive manufacturing technique. The ceramic suspension should have sufficient flowability for precision casting and machinability. Furthermore, high solids volume fraction is crucial for achieving sufficient strength. When the ceramic suspension has a high solid volume fraction, aggregation of the ceramic particles and the high shear

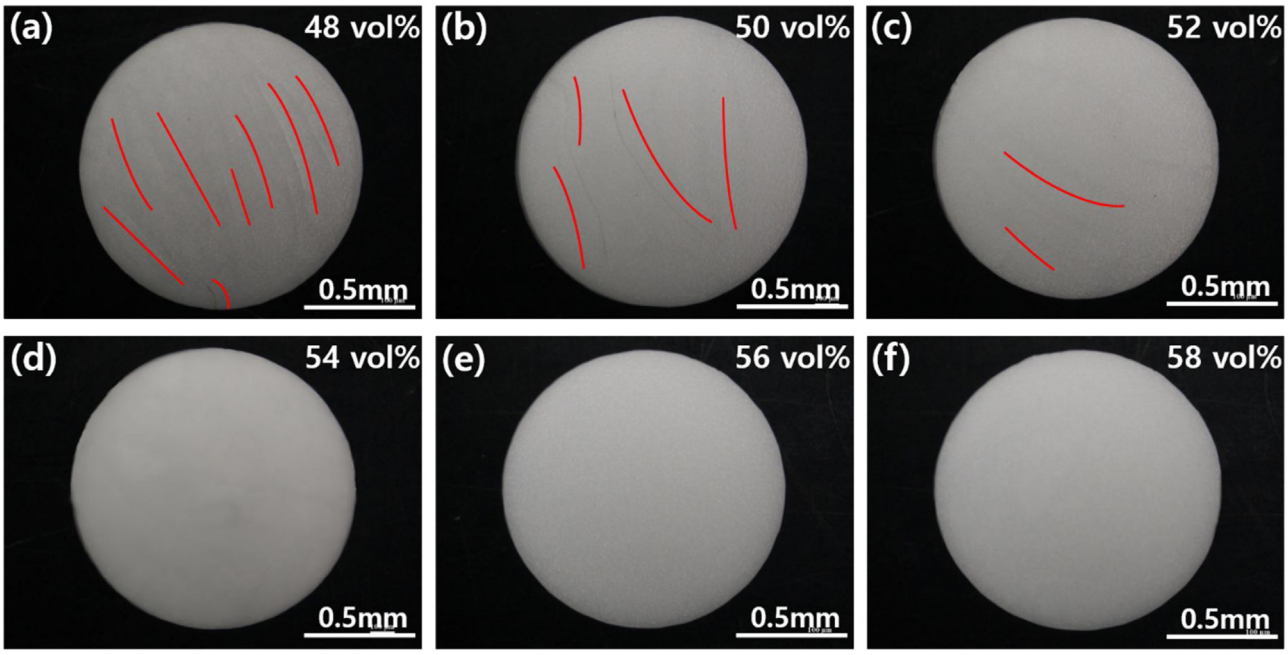

Fig. 12 – The top view of the sintered specimens for different volume fraction of zirconia; red lines mark the minor cracks on the surface of zirconia specimens.

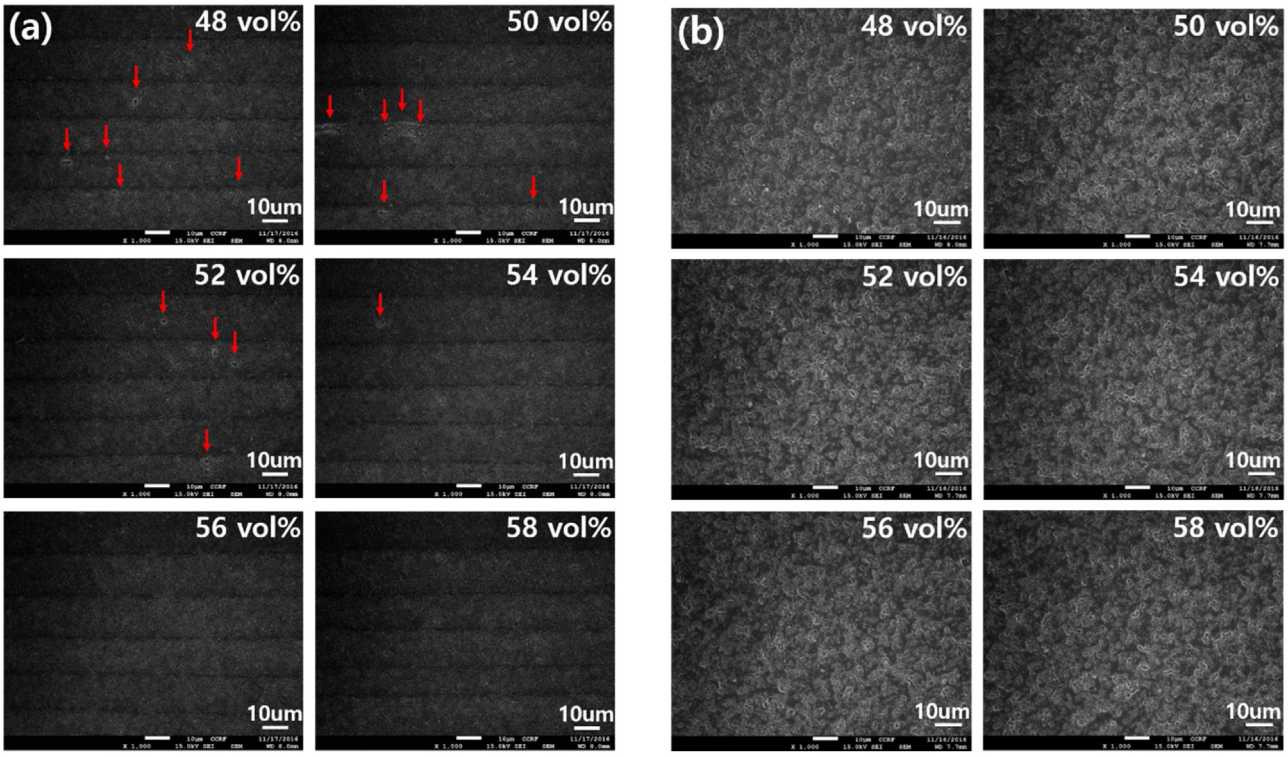

Fig. 13 – Cross-sectional SEM images for different volume fractions of zirconia. (A) Green body specimens. The red arrows show defects that appeared when the zirconia volume fraction decreased. (B) Sintered specimens.

stress of the suspension are problems to be solved. Compromised dispersibility of the ceramic suspensions leads to defects in the final product. The ceramic suspensions for ceramic additive manufacturing must have sufficient flowability through effective dispersion even at high solid volume fraction. Aggregation can be controlled by hydrodynamic effects from the flow of photo polymers around the zirconia particles. For a suspension containing significant amounts of

solid components, the viscosity of a suspension of volume fraction (∅) can be explained by the Krieger–Dougherty equation [33].

$$\eta_r = \frac{\eta(\emptyset)}{\eta_0} = \left(1 - \frac{\emptyset}{\emptyset_0}\right)^{-n} \quad (1)$$

Here, η_r is the relative viscosity of the suspension, η_0 is the viscosity coefficient of the medium, and $\emptyset_0$ is the limit of the Krieger model. The correlation between solid content and viscosity can be explained by the function of volume fraction and the relative viscosity in Eq. (1). As the particle volume fraction approached the maximum volume fraction or packing fraction, $\emptyset_m$, the viscosity of the suspension was drastically increased. Therefore, the viscosity of the suspension could be reduced for a given ∅ by increasing the maximum volume fraction, $\emptyset_m$.

Based on this theory, Griffith has suggested an upper limit of 3000 m Pa s for viscosity of a suspension in SLA-based additive manufacturing techniques [34]. He also reported that as the ceramic particle size increased from 0.3 μm to 40 μm, the maximum volume fraction of ceramic increased from 49 to 62% and this change in the particle size distribution can increase the maximum volume fraction of ceramic in suspension. And the maximum volume fraction of ceramic might also be increased by the type of dispersant and diluent. It may also vary depending on the influence of packing factors. For this reason, it is very important to increase the dispersibility of the suspension using optimized materials.

The energy of the UV light source and the curing time can affect the properties of products and bonding strength of repeat layers. Layers of a solid object are stacked in accordance with the preset thickness. If the photocuring cure depth is not enough, delamination between layers might occur, leading to defects that can significantly affect the physical properties of the sintered product. Therefore, photocuring ability is important for sufficient bonding strength between layers to prevent defects in products. In this experiment, the thickness of 25 μm per layer was preset and the cure depth was 50 μm after 1 s of photocuring (Fig. 5). Since the cure depth was twice the preset thickness of a layer, the degree of photocuring in this experiment is considered appropriate for use. Factors affecting the cure depth can be explained according to Jacob's equation of the Beer–Lambert law in terms of resin sensitivity (D_P) and threshold energy [35].

$$C_d = D_P \ln\left(\frac{E}{E_C}\right) \quad (2)$$

In this equation, C_d is the absolute cure depth, D_P is the resin sensitivity indicating the distance at which the laser intensity is decreased by 1/e, E_C is the threshold energy at which the resin would harden, and E is the surface energy density. The sensitivity of the photocuring resin in the suspension depends on the volume fraction, particle size, and refractive index of zirconia according to Eq. (2). During the photopolymerization process, multiple scattering of light from each material can result in geometrical overgrowth due to the different refractive indexes of materials. The incident light will be scattered more by the zirconia particles that are added to acrylic monomers in the suspension [36,37]. This scattering effect would be affected by solids volume and difference in refractive index between zirconia and the solvent.

The polymers should be successfully removed by the debinding process as a prerequisite for sintering. The inappropriate debinding process can lead to blistering, cracks, and delamination. Thermogravimetric analysis (TG-DTA) is an effective method to obtain the heat processing step and dwell time for the debinding process. Organic compounds are gradually removed in corresponding temperature ranges depending on the functional groups of polymers in the polymer mixture. All organic binders were removed below 600 °C. and printed zirconia specimens were sintered at 1450 °C. Careful cooling of specimens was necessary to prevent cracks caused by drastic contraction and thermal shock.

There are three types of mass transfer mechanisms during sintering: surface diffusion, evaporation–condensation, and volume diffusion [38]. During surface diffusion, a common transfer mechanism, surface smoothing, particle joining, and pore rounding will be produced. During evaporation–condensation, sublimation and vapor transferring from a relatively high vapor pressure surface to a low vapor pressure surface might occur according to the radius of the particle's curvature. During volume diffusion, necking growth and volume contraction might occur through the lattice and along the grain boundaries of zirconia particles. While surface diffusion and evaporation–condensation do not have significant densification effects, diffusion along the particle grain boundaries can induce densification during the process of reduction of the surface area [39].

The relative density increased as the volume fraction increased. Relative density was 92.79% and the bending strength was 674.74 MPa with a corresponding linear shrinkage rate of 19.37% for a volume fraction of 58%. A volume fraction of 58% was the maximum volume fraction of zirconia possible for printing in this experiment. Photo polymers and dispersants within the solid product acted as impurities and might have formed porous structures during the debinding and sintering processes, thus affecting the bending strength. In a study, glass infiltration improved strength by compensating for these fine pores [40].

Phase transformations due to the high sintering temperature resulted in the presence of tetragonal phases in all specimens. The monoclinic phase was not detected. It seems that cracking on the surfaces of sintered zirconia was caused by insufficient necking between zirconia particles in samples with low zirconia volume fraction. No cracks were observed in volume fractions higher than 54 vol%.

5. Conclusion

The effect of the volume fraction of zirconia suspension on the physical properties and microstructure of products fabricated by additive manufacturing was studied. In this experiment, the zirconia suspension showed a sharp increase in viscosity above 54 vol% and 58 vol% was the maximum volume fraction possible for 3D printing. After photocuring of 15 s, sufficient

cure depth could be obtained in all groups but the cure depth deceased as volume fraction increased.

The bending strength ranged from a minimum of 94 MPa (48 vol%) to a maximum of 674 MPa (58 vol%) depending on the volume fraction of zirconia. The geometrical overgrowth by light scattering ranged from a minimum of 28.55% to a maximum of 36.94%.

Precision and bending strength are the problems to be overcome in the future for further application of zirconia additive manufacturing.

Funding

This work was supported by a National Research Foundation of Korea (NRF) grant funded by the Korean government (MSIP) [No. 2015R1A2A2A01008148]. The funder had no role in study design, in the collection, analysis and interpretation of data, in the writing of the report; and in the decision to submit the article for publication.

REFERENCES

[1] Sundh A, Sjögren G. A study of the bending resistance of implant-supported reinforced alumina and machined zirconia abutments and copies. Dent Mater 2008;24(5):611–7.
[2] Wang H, Aboushelib MN, Feilzer AJ. Strength influencing variables on CAD/CAM zirconia frameworks. Dent Mater 2008;24(5):633–8.
[3] Denry I, Kelly JR. State of the art of zirconia for dental applications. Dent Mater 2008;24(3):299–307.
[4] Preis V, Behr M, Handel G, Schneider-Feyrer S, Hahnel S, Rosentritt M. Wear performance of dental ceramics after grinding and polishing treatments. J Mech Behav Biomed Mater 2012;10:13–22.
[5] Preis V, Behr M, Hahnel S, Handel G, Rosentritt M. In vitro failure and fracture resistance of veneered and full-contour zirconia restorations. J Dent 2012;40(11):921–8.
[6] Dawood A, Marti BM, Sauret-Jackson V, Darwood A. 3D printing in dentistry. Br Dent J 2015;219(11):521.
[7] Madhav VNV, Daule R. Rapid prototyping and its application in dentistry. J Dent Allied Sci 2013;2(2):57–61.
[8] Schwentenwein M, Schneider P, Homa J. Lithography-based ceramic manufacturing: A novel technique for additive manufacturing of high-performance ceramics. Adv Sci Technol 2014;88:60–4.
[9] Song X, Chen Y, Lee TW, Wu S, Cheng L. Ceramic fabrication using Mask-Image-Projection-based Stereolithography integrated with tape-casting. J Manuf Process 2015;20:456–64.
[10] Wu H, Cheng Y, Liu W, He R, Zhou M, Wu S, et al. Effect of the particle size and the debinding process on the density of alumina ceramics fabricated by 3D printing based on stereolithography. Ceramics Int 2016;42(15):17290–4.
[11] Halloran JW. Ceramic stereolithography additive manufacturing for ceramics by photopolymerization. Annu Rev Mater Res 2016;46:19–40.
[12] Ebert J, Ozkol E, Zeichner A, Uibel K, Weiss O, Koops U, et al. Direct inkjet printing of dental prostheses made of zirconia. J Dent Res 2009;88(7):673–6.
[13] Bae CJ. Integrally cored ceramic investment casting mold fabricated by ceramic stereolithography. [Dissertation]. ProQuest; 2008.
[14] Shahzad K, Deckers J, Zhang Z, Kruth J, Vleugels J. Additive manufacturing of zirconia parts by indirect selective laser sintering. J Eur Ceram Soc 2014;34(1):81–9.
[15] Mitteramskogler G, Gmeiner R, Felzmann R, Gruber S, Hofstetter C, Stampfl J, et al. Light curing strategies for lithography-based additive manufacturing of customized ceramics. Addit Manuf 2014;1:110–8.
[16] Hinczewski C, Corbel S, Chartier T. Ceramic suspension suitable for stereolithography. J Eur Ceram Soc 1998;18(6):583–90.
[17] Chartier T, Chaput C, Doreau F, Loiseau M. Stereolithography of structural complex ceramic parts. J Mater Sci 2002;37(15):3141–7.
[18] Johansson Emil Lidström O, Johansson J, Lyckfeldt O, Adolfsson E. Influence of resin composition on the defect formation in alumina manufactured by stereolithography. Materials 2017;10(2):138.
[19] Kambly K. Characterization of curing kinetics and polymerization shrinkage in ceramic-loaded photocurable resins for large area maskless photopolymerization (LAMP). [Dissertation]. Georgia Institute of Technology; 2009.
[20] Bae CJ, Halloran JW. Integrally cored ceramic mold fabricated by ceramic stereolithography. Int J Appl Ceram Tech 2011;8(6):1255–62.
[21] Bae CJ, Halloran JW. Influence of residual monomer on cracking in ceramics fabricated by stereolithography. Int J Appl Ceram Tech 2011;8(6):1289–95.
[22] Griffith ML, Halloran JW. Freeform fabrication of ceramics via stereolithography. J Am Ceram Soc 1996;79(10):2601–8.
[23] Halloran JW , Griffith M, Chu TM, Stereolithography resin for rapid prototyping of ceramics and metals. U.S. Patent No. 6,117,612. 12 September 2000.
[24] Tay BY, Evans JRG, Edirisinghe MJ. Solid freeform fabrication of ceramics. Int Mater Rev 2013:341–70.
[25] Schwentenwein M, Homa J. Additive manufacturing of dense alumina ceramics. Int J App Ceram Technol 2015;12(1):1–7.
[26] Jang KJ, Kang JH, Sakthiabirami K, Lim HP, Yun KD, Yim EK, et al. Evaluation of cure depth and geometrical overgrowth depending on zirconia volume fraction using digital light processing. J Nanosci Nanotechnol 2019;19(4):2154–7.
[27] ISO 2555. Plastics – resins in the liquid state or as emulsions or dispersions – determination of apparent viscosity by the Brookfield test method; 1989.
[28] ISO 11358-1. Plastics – thermogravimetry (TG) of polymers – part 1: general principles; 2014.
[29] ASTM, ASTM. C326 — Test method for drying and firing shrinkage of ceramic whiteware clays. American Society for Testing and Materials; 1997.
[30] ISO 18754. Fine ceramics (advanced ceramics, advanced technical ceramics) — determination of density and apparent porosity; 2013.
[31] ISO 6872. Dentistry — ceramic materials; 2015.
[32] ISO 13356. Implants for surgery — ceramic materials based on yttria-stabilized tetragonal zirconia (Y-TZP); 2015.
[33] Krieger IM, Dougherty TJ. A mechanism for non-Newtonian flow in suspension of rigid spheres. Trans Soc Rheol (1957–1977) 1959;3:137–52.
[34] Griffith ML. Stereolithography of ceramics. [Dissertation]. University of Michigan; 1995.
[35] Jacobs PF. Rapid prototyping & manufacturing: fundamentals of stereolithography. Society of Manufacturing Engineers: Dearborn, MI; 1992.
[36] Gentry SP, Halloran JW. Light scattering in absorbing ceramic suspensions: effect on the width and depth of photopolymerized features. J Eur Ceram Soc 2015;35(6):1895–904.

[37] Griffith ML, Halloran JW. Scattering of ultraviolet radiation in turbid suspension. J Appl Phys 1997;81(6):2538–46.
[38] Brady GA, Halloran JW. Differential photo-calorimetry of photopolymerizable ceramic suspension. J Mater Sci 1998;33(18):4551–60.
[39] Odian G. Principles of polymerization. Hoboken, NJ: John Wiley & Sons; 2004.
[40] Park SW, Oh GJ, Jang MK, Ji MK, Kim JH, Kim JW, et al. Effect of infiltration with ferric oxide containing glass on the color and mechanical properties of zirconia. Key Eng Mater 2016;696:113–7.